

## Enhancement of CO<sub>2</sub> Uptake and Selectivity in a Metal–Organic Framework by the Incorporation of Thiophene Functionality

Vsevolod A. Bolotov,<sup>†</sup> Konstantin A. Kovalenko,<sup>†,‡</sup> Denis G. Samsonenko,<sup>†,‡</sup> Xue Han,<sup>§</sup> Xinran Zhang,<sup>§</sup> Gemma L. Smith,<sup>§</sup> Laura J. McCormick,<sup>||</sup> Simon J. Teat,<sup>||</sup> Sihai Yang,<sup>§</sup> Matthew J. Lennox,<sup>⊥,#</sup> Alice Henley,<sup>#</sup> Elena Besley,<sup>#</sup> Vladimir P. Fedin,<sup>†,‡</sup> Danil N. Dybtsev,<sup>\*,†,‡</sup> and Martin Schröder<sup>\*,†,‡,§</sup>

<sup>†</sup>Nikolaev Institute of Inorganic Chemistry (NIIC), Siberian Branch of the Russian Academy of Sciences, 3 Ac. Lavrentiev Avenue, Novosibirsk 630090, Russian Federation

<sup>‡</sup>Novosibirsk State University, 2 Pirogova Street, Novosibirsk 630090, Russian Federation

<sup>§</sup>School of Chemistry, University of Manchester, Manchester M13 9PL, U.K.

<sup>||</sup>Advanced Light Source, Lawrence Berkeley National Laboratory, Berkeley, California 94720, United States

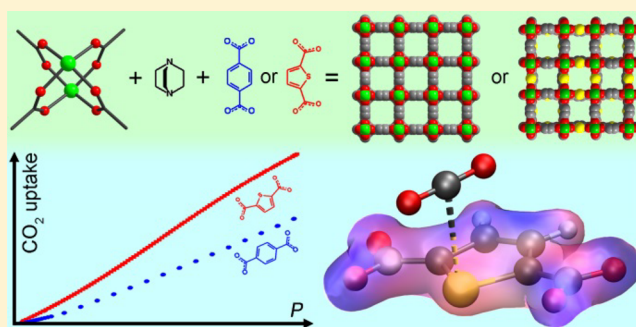
<sup>⊥</sup>Centre for Advanced Separations Engineering, Department of Chemical Engineering, University of Bath, Bath BA2 7AY, U.K.

<sup>#</sup>School of Chemistry, University of Nottingham, Nottingham NG7 2RD, U.K.

### **S** Supporting Information

**ABSTRACT:** The complex [Zn<sub>2</sub>(tdc)<sub>2</sub>dabco] (H<sub>2</sub>tdc = thiophene-2,5-dicarboxylic acid; dabco = 1,4-diazabicyclooctane) shows a remarkable increase in carbon dioxide (CO<sub>2</sub>) uptake and CO<sub>2</sub>/dinitrogen (N<sub>2</sub>) selectivity compared to the nonthiophene analogue [Zn<sub>2</sub>(bdc)<sub>2</sub>dabco] (H<sub>2</sub>bdc = benzene-1,4-dicarboxylic acid; terephthalic acid). CO<sub>2</sub> adsorption at 1 bar for [Zn<sub>2</sub>(tdc)<sub>2</sub>dabco] is 67.4 cm<sup>3</sup>·g<sup>-1</sup> (13.2 wt %) at 298 K and 153 cm<sup>3</sup>·g<sup>-1</sup> (30.0 wt %) at 273 K. For [Zn<sub>2</sub>(bdc)<sub>2</sub>dabco], the equivalent values are 46 cm<sup>3</sup>·g<sup>-1</sup> (9.0 wt %) and 122 cm<sup>3</sup>·g<sup>-1</sup> (23.9 wt %), respectively. The isosteric heat of adsorption for CO<sub>2</sub> in [Zn<sub>2</sub>(tdc)<sub>2</sub>dabco] at zero coverage is low (23.65 kJ·mol<sup>-1</sup>), ensuring facile regeneration of the porous material.

Enhancement by the thiophene group on the separation of CO<sub>2</sub>/N<sub>2</sub> gas mixtures has been confirmed by both ideal adsorbate solution theory calculations and dynamic breakthrough experiments. The preferred binding sites of adsorbed CO<sub>2</sub> in [Zn<sub>2</sub>(tdc)<sub>2</sub>dabco] have been unambiguously determined by in situ single-crystal diffraction studies on CO<sub>2</sub>-loaded [Zn<sub>2</sub>(tdc)<sub>2</sub>dabco], coupled with quantum-chemical calculations. These studies unveil the role of the thiophene moieties in the specific CO<sub>2</sub> binding via an induced dipole interaction between CO<sub>2</sub> and the sulfur center, confirming that an enhanced CO<sub>2</sub> capacity in [Zn<sub>2</sub>(tdc)<sub>2</sub>dabco] is achieved without the presence of open metal sites. The experimental data and theoretical insight suggest a viable strategy for improvement of the adsorption properties of already known materials through the incorporation of sulfur-based heterocycles within their porous structures.



### INTRODUCTION

Carbon dioxide (CO<sub>2</sub>) release poses one of the biggest anthropogenic impacts to the environment. While broad implementation of low-carbon fuels and strategies will reduce CO<sub>2</sub> release, power plants, cement, and steel production represent major industries that will continue to generate exhausts that require effective purification to remove CO<sub>2</sub> as well as other harmful gases.<sup>1</sup> CO<sub>2</sub> sequestration through selective adsorption is viewed as one of the most promising approaches because of its simple implementation, the absence of hazardous materials, tunable selectivity, and low energy costs.<sup>2</sup> Thus, porous materials, such as metal–organic frameworks (MOFs), with the highest CO<sub>2</sub> adsorption capacity at relatively low partial pressures (<5 bar) are valuable targets for such applications.<sup>3–10</sup> High adsorption selectivity and high

uptake under ambient conditions may be enhanced in porous materials by the incorporation of specific binding sites at the pore surface. The main strategies for the incorporation of CO<sub>2</sub> binding centers into MOF structures have been via the incorporation of basic centers such as amines functioning as Lewis bases<sup>11–15</sup> and adsorption at coordinatively unsaturated metal cations as Lewis acid sites.<sup>16–21</sup> The former strategy is a development of the traditional approach of CO<sub>2</sub> capture by amines to form carbamates and shows high uptake and very good adsorption selectivity even under humid conditions but also, significantly, increases the energy cost for regeneration of the adsorbate. The latter strategy employs CO<sub>2</sub> binding

Received: January 15, 2018

Published: April 23, 2018

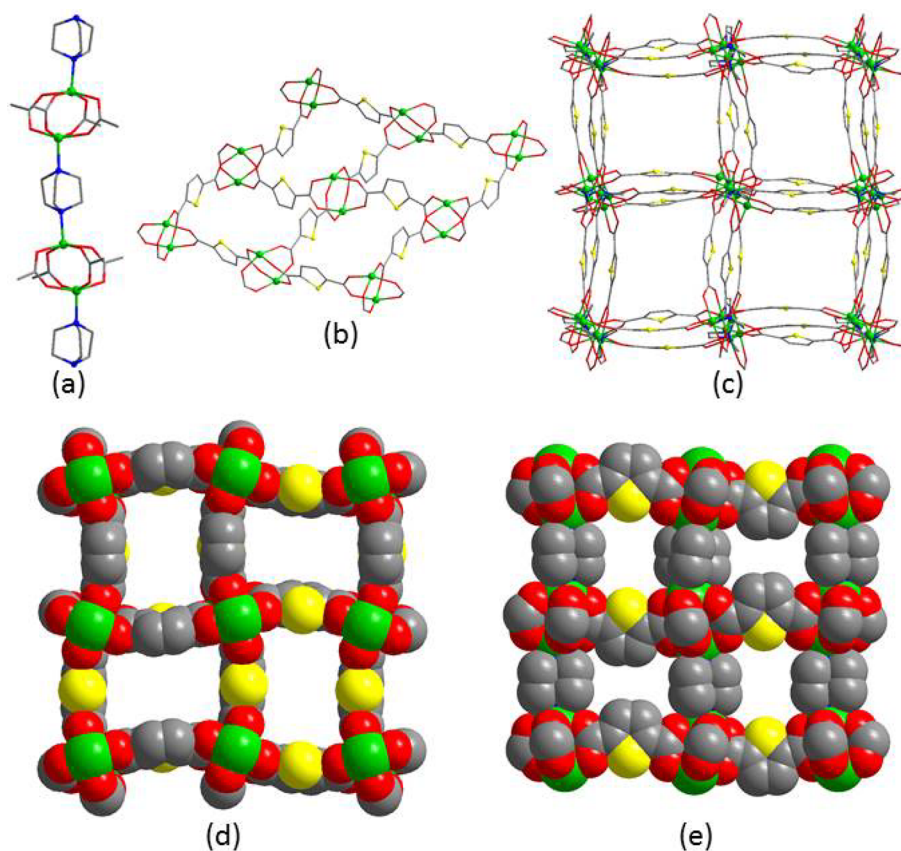


**Figure 1.** Views of structure of the as-synthesized **1**: view of the  $[\text{Zn}_2(\text{OOCR})_4]$  paddlewheels, connected by dabco ligands (a); structure of the  $[\text{Zn}_2(\text{tdc})_2]$  layer (b); projection of the crystal structure of **1** along the 4-fold axis (c); aperture of the channels along the 4-fold axis (d); aperture of the channels across the 4-fold axis (e). Color code: Zn, green; S, yellow; O, red; N, blue; C, gray. Hydrogen atoms are not shown.

through interaction to vacant metal sites. Despite a number of advantages such as a moderate energy penalty for regeneration and tunability of the adsorption sites, such materials often only function under strictly anhydrous conditions as water competes effectively for binding at the unsaturated metal sites. Also, the open metal sites usually reach saturation rapidly and thus lose their activity in selective guest binding. Because each strategy has its particular disadvantages, the development of porous materials with high adsorption selectivity and appreciable  $\text{CO}_2$  uptake under ambient conditions capable of working under humid environments and possessing a low regeneration penalty requires new approaches based on other types of inter- and supramolecular interactions. With a handful of exceptions,<sup>19,22–32</sup> weak van der Waals and supramolecular interactions have not been widely considered as a driving force for specific  $\text{CO}_2$  binding, which could result in appreciable adsorption selectivity and improved storage capacity. We demonstrate herein that the incorporation of thiophene moieties with polarizable sulfur heteroatoms, capable of induced dipole–dipole interactions, results in a remarkable increase of the  $\text{CO}_2$  binding affinity of the microporous MOF  $[\text{Zn}_2(\text{tdc})_2\text{dabco}]$  ( $\text{H}_2\text{tdc}$  = thiophene-2,5-dicarboxylic acid; dabco = 1,4-diazabicyclooctane). This increases both the storage capacity and selectivity of the framework at ambient conditions by as much as 50%, in a comparison of thiophene with phenyl functionalization, and also maintains the heat of adsorption at a low level to minimize penalty costs for regeneration. The enhanced  $\text{CO}_2$  binding property of the thiophene-containing MOF has also been confirmed by fixed-

bed breakthrough separation of a  $\text{CO}_2/\text{N}_2$  mixture. More importantly, adsorbed  $\text{CO}_2$  molecules within  $[\text{Zn}_2(\text{tdc})_2\text{dabco}]$  have been directly observed and quantified by in situ single-crystal diffraction experiments, revealing the preferential host–guest binding interaction in the pores. The mechanism of MOF– $\text{CO}_2$  binding has also been studied by quantum-chemical calculations, giving detailed insight into the role of the sulfur atoms in  $\text{CO}_2$  supramolecular binding. These results provide a new viable strategy underpinning the development of MOF materials with improved uptake and selectivity for  $\text{CO}_2$ .

## ■ MATERIALS AND METHODS

All chemicals were of analytical grade and were used without additional purification. *N,N*-Dimethylformamide (DMF) was dried over activated molecular sieves (3 Å) prior to use.

**Synthesis of  $[\text{Zn}_2(\text{tdc})_2\text{dabco}]\cdot 4\text{DMF}$  (**1**).** To a mixture of  $\text{Zn}(\text{NO}_3)_2\cdot 6\text{H}_2\text{O}$  (120 mg, 404  $\mu\text{mol}$ ) and thiophene-2,5-dicarboxylic acid ( $\text{H}_2\text{tdc}$ ; 47 mg, 273  $\mu\text{mol}$ ) in DMF (5.3 mL) was added dropwise dabco (23 mg, 205  $\mu\text{mol}$ ) in DMF (4.0 mL) under rigorous stirring to avoid the formation of any precipitate. The resulting clear solution was heated at 100 °C for 20 h. The colorless block-shaped crystals were collected and washed with DMF. Yield: 0.093 mg (78% based on  $\text{H}_2\text{tdc}$ ). Elem. anal. Calcd for  $1\cdot\text{H}_2\text{O}$ : C, 40.3; H, 5.2; N, 9.4; S, 7.2. Found: C, 40.4; H, 5.0; N, 9.2; S, 7.4. TGA. Calcd for 4DMF: 33.4%. Found: 30.5%. FT-IR (KBr,  $\nu_{\text{C=O}}$  of DMF): 1667  $\text{cm}^{-1}$ .

The synthesis of  $[\text{Zn}_2(\text{tdc})_2\text{bpe}]\cdot 2\text{DMF}$  [**2**; bpe = 1,2-bis(4-pyridyl)ethane] and  $[\text{Zn}_2(\text{tdc})_2\text{bpp}]\cdot 2\text{DMF}$  [**3**; bpp = 1,3-bis(4-pyridyl)propane] was carried out using a similar procedure starting from  $\text{Zn}(\text{NO}_3)_2\cdot 6\text{H}_2\text{O}$  (250 mg, 842  $\mu\text{mol}$ ),  $\text{H}_2\text{tdc}$  (145 mg, 843  $\mu\text{mol}$ ), and either bpe (75 mg, 408  $\mu\text{mol}$ ) or bpp (84 mg, 424  $\mu\text{mol}$ ). The corresponding solids were dissolved in DMF (10 mL) with

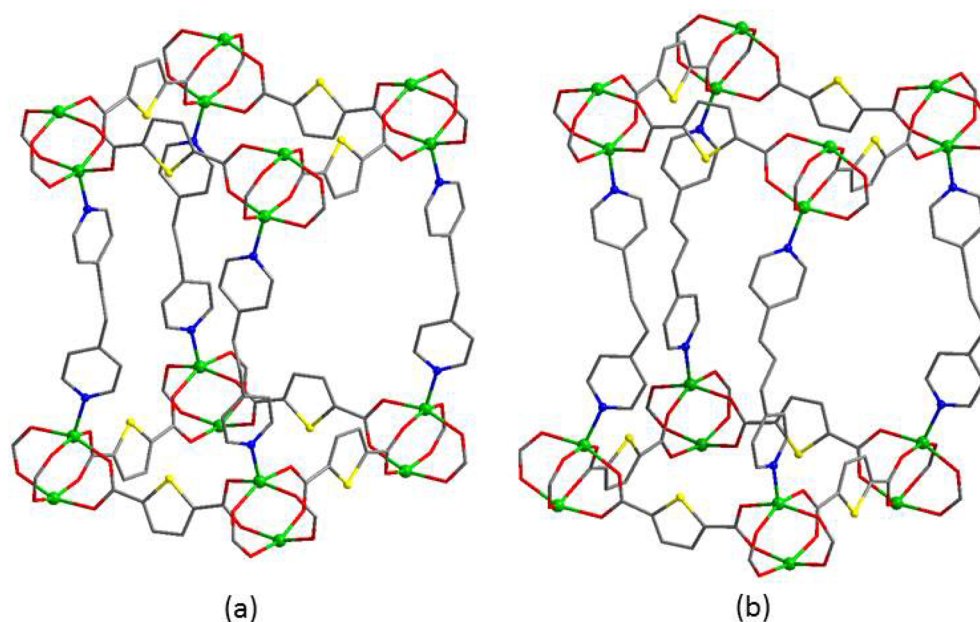


**Figure 2.** Views of the single nets of  $2^{33}$  (a) and  $3$  (b). Color code: Zn, green; S, yellow; O, red; N, blue; C, gray. Hydrogen atoms are not shown.

rigorous stirring and sonification. An unknown precipitate was removed from the reaction solution by centrifugation and the clear solution heated at 100 °C for 40 h. Block-shaped crystals of the product were collected and washed in DMF. The yields were 236 mg (69%) for **2** and 263 mg (73%) for **3**. Elem anal. Calcd for **2**: C, 45.0; H, 3.8; N, 7.0; S, 8.0. Found: C, 45.0; H, 3.9; N, 7.0; S, 7.8. Calcd for **3**: C, 45.7; H, 4.0; N, 6.9; S, 7.9. Found: C, 45.3; H, 3.9; N, 6.8; S, 7.5. TGA for **2**. Calcd for 2DMF: 18.3%. Found: 17.8%. TGA for **3**. Calculated for 2DMF: 18.0%. Found: 17.4%. FT-IR (KBr,  $\nu_{C=O}$  of DMF): **2**, 1675  $\text{cm}^{-1}$ ; **3**, 1666  $\text{cm}^{-1}$ .

**Synthesis of Activated  $[\text{Zn}_2(\text{tdc})_2\text{dabco}]$  (**1a**).** The as-synthesized compound **1** was heated at 90 °C in vacuo for 10 h. The sample weight loss was 30.3%. Elem anal. Calcd for **1a**· $\text{H}_2\text{O}$ : C, 36.0; H, 3.0; N, 4.7; S, 10.7. Found: C, 36.2; H, 3.0; N, 4.8; S, 10.9.

**Synthesis of Activated  $[\text{Zn}_2(\text{tdc})_2\text{bpe}] \cdot 2\text{DMF}$  (**2**) and  $[\text{Zn}_2(\text{tdc})_2\text{bpp}] \cdot 2\text{DMF}$  (**3**).** The as-synthesized crystals of **2** and **3** were heated at 100 °C in vacuo for 6 h. The sample weight losses were found to be 18.4% for **2** and 17.7% for **3**. Elem anal. Calcd for **2**: C, 44.0; H, 2.5; N, 4.3; S, 9.8. Found: C, 43.7; H, 2.4; N, 4.2; S, 9.5. Calculated for  $3 \cdot \frac{2}{3}\text{H}_2\text{O}$ : C, 44.1; H, 2.9; N, 4.1; S, 9.4. Found: C, 44.5; H, 2.7; N, 4.2; S, 9.0.

## RESULTS AND DISCUSSION

**Synthesis and Crystal Structure Analysis.** The coordination polymer **1** was prepared by the solvothermal reaction of  $\text{Zn}(\text{NO}_3)_2$ ,  $\text{H}_2\text{tdc}$ , and dabco in hot DMF (100 °C) to give rectangular colorless single crystals. The stability of **1** was found to be very similar to that of many zinc(II) carboxylate MOFs. The crystalline material **1** is stable in organic media but decomposes rapidly in water. The as-synthesized crystals **1** can be handled in air for several hours without any impact on the crystallinity. Single-crystal X-ray diffraction confirms that **1** crystallizes in the tetragonal space group  $P4_21c$  and incorporates binuclear paddlewheel nodes  $[\text{Zn}_2(\text{OOCR})_4]$  (Figure 1a) bound by four carboxylate groups of  $\text{tdc}^{2-}$  anions to form a slightly squeezed layer of square-grid topology with a corrugated overall structure (Figure 1b). The remaining available coordination site at the square-pyramidal zinc(II) cations are bound by nitrogen-atom donors of the dabco ligands, which connect  $[\text{Zn}_2(\text{tdc})_2]$  layers into a 3D porous framework with a scaffoldlike primitive cubic topology pcu

(Figure 1c). Rotation of the dabco ligands results, as expected, in severe disorder of the carbon atoms of the  $\text{CH}_2\text{CH}_2$  moieties, and the rigid angular shape of the  $\text{tdc}^{2-}$  anion forces notable distortions of the paddlewheel unit such that the Zn–Zn axis is twisted from the  $c$  crystallographic direction of the unit cell by ca. 16°. The van der Waals aperture of the channels running along the 4-fold axis is  $5 \times 8$  Å, corresponding to the shape of the squeezed square window of the  $[\text{Zn}_2(\text{tdc})_2]$  layer (Figure 1d). These corrugated layers stack along the  $c$  direction in an alternating ABAB fashion, forming two different types of smaller windows across the 4-fold axis. The narrower window has van der Waals dimensions of  $2.5 \times 5$  Å formed by two closely located  $\text{tdc}^{2-}$  moieties. The wider  $3.5 \times 5$  Å window is formed by two  $\text{tdc}^{2-}$  arcs bent outward from each other with an interatomic S··S distance of 8.5 Å (Figure 1e). It is worth noting that the slight tilting of the thiophene groups [i.e., the orientation of the heteroatom (vide supra)] results in two different types of pore environments (Figure 1b). Regardless of this tilting, both types of channels have similar apertures and are set up for the diffusion of gas molecules with potential interaction with the sulfur atoms of the thiophene moieties.

In a similar manner, two additional microporous zinc(II) thiophene-2,5-dicarboxylates, **2** and **3**, were synthesized using 1,2-bis(4-pyridyl)ethane (bpe) and 1,3-bis(4-pyridyl)propane (bpp) as nitrogen-donor bridging ligands, respectively. During the course of this work, the synthesis and structure of **2** were reported.<sup>33</sup> In **2** and **3**, the structure of the  $[\text{Zn}_2(\text{tdc})_2]$ -corrugated layer remains unchanged compared to **1**, and these layers are connected through longer N-donor linkers (Figure 2). Elongation of the bridging ligand does open up the possibility for framework interpenetration, which is not possible for **1** incorporating shorter dabco ligands.<sup>34</sup> As a result, structure **1** is a single noninterpenetrated net, while **2** and **3** show doubly interwoven structures with pcu topology. Despite interpenetration, both **2** and **3** contain microporous volume filled with solvent molecules in the as-synthesized materials. We should also note that, in spite of our numerous attempts to obtain similar structures with 4,4'-bipyridyl or *trans*-bis(4-pyridyl)ethylene bridging ligands, we could not crystallize any

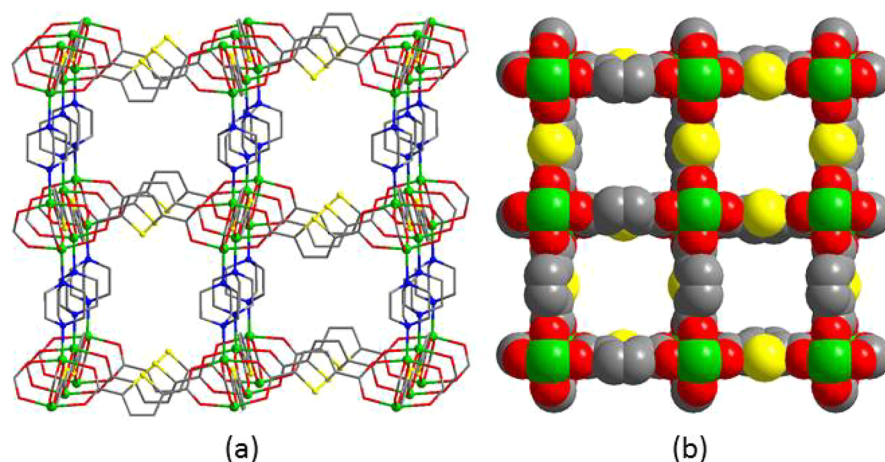


**Figure 3.** Views of the crystal structure of **1a**: wireframe presentation viewed along the  $[\text{Zn}_2(\text{tdc})_2]$  layers (a); van der Waals model view along the 4-fold axis (b). Color code: Zn, green; S, yellow; O, red; N, blue; C, gray. Hydrogen atoms are not shown.

product thus far. The problem could be related to steric constraint of the substantially skewed  $[\text{Zn}_2(\text{OOCR})_4]$  paddle-wheel building units, which cannot be interconnected by structurally rigid linear ligands. Dabco is an apparent exception because of its aliphatic nature and the formation of rather strong metal–ligand coordination bonds. The micropores of the as-synthesized materials **1–3** are filled by DMF solvent molecules, which were located from the X-ray diffraction data. The FT-IR spectra and chemical and thermogravimetric analyses confirm the nature and composition of the guest molecules. According to the TGA data, the DMF molecules can be removed by heating the material to 170–190 °C, while the irreversible thermolysis of the MOF takes place near 300 °C for **1** and **2** or 330 °C for **3**.

The guest-free sample **1a** was obtained by thermal activation of the as-synthesized crystals **1** in vacuo. Compared with the as-synthesized **1**, the activated **1a** is more susceptible to airborne moisture, but no sign of degradation of the powder X-ray diffraction (PXRD) pattern or gas adsorption properties was observed for **1a** exposed to air for 1 h. The crystalline material was sufficiently robust to sustain the activation procedure, so we were able to characterize the solvent-free open structure **1a** by single-crystal X-ray diffraction. The space group was found to be  $I4/mmm$  (tetragonal), and the local coordination of the metal cations as well as the overall pcu connectivity remained unchanged from **1** (Figure 3a). The only notable difference is that the anionic  $\text{tdc}^{2-}$  linkers are more linear in the guest-free structure **1a**, resulting in a higher symmetry and a more regular structure with rectangular channels of van der Waals aperture,  $6.5 \times 6.5 \text{ \AA}$  (Figure 3b). This straightening of the organic ligands results in an overall expansion of the guest-free structure **1a**, compared to the solvated material **1**. The total unit cell volume increases during the activation by ca. 3%. Notably, the structural changes between **1** and **1a** are fully reversible because the guest-free compound **1a** shrinks back when placed in DMF solvent to reform **1**. It is worth noting that the analogous compound based on terephthalate  $\text{bdc}^{2-}$  bridging ligands  $[\text{Zn}_2(\text{bdc})_2\text{dabco}] \cdot \text{xsolv}$  (**4**) features the same reversible structural changes upon framework activation and resolution, although the degree of volume expansion/contraction of the unit cell in **4** is somewhat greater (3–5%) depending on the nature of the solvent.<sup>35,36</sup>

**Gas Adsorption Studies.** Activation of the interpenetrated compounds **2** and **3** was achieved by heating the compounds in

vacuo at 100 °C for 6 h. Complete removal of the guest DMF molecules without framework collapse was confirmed by PXRD, TGA, chemical analyses, and IR spectroscopy. Some shifting of the PXRD peaks to higher  $2\theta$  angles upon desolvation of **3** indicates shrinkage of the partially flexible framework.  $\text{N}_2$  adsorption measurements for the activated samples at 77 K showed reversible type I isotherms, characteristic of microporous materials, with pore volumes of 0.19 and 0.20  $\text{cm}^3 \cdot \text{g}^{-1}$  and BET surface areas of 447 and 407  $\text{m}^2 \cdot \text{g}^{-1}$  for **2** and **3**, respectively (see the Supporting Information). The relatively low porosity for these compounds is not surprising given the observed 2-fold-interpenetrated structures for these species.

The stability and permanent porosity of the guest-free compound **1a** were confirmed by PXRD and gas adsorption measurements. The  $\text{N}_2$  isotherm at 77 K reveals a type I reversible isotherm (Figure 4) with a pore volume of 0.68  $\text{cm}^3 \cdot \text{g}^{-1}$  and a BET surface area of 1553  $\text{m}^2 \cdot \text{g}^{-1}$ . The pore volume is similar to the expected value of 0.63  $\text{cm}^3 \cdot \text{g}^{-1}$  calculated from the gravimetric density of the framework **1a** (0.94  $\text{g} \cdot \text{cm}^{-3}$ ) and its guest accessible volume (0.59 v/v) according to the

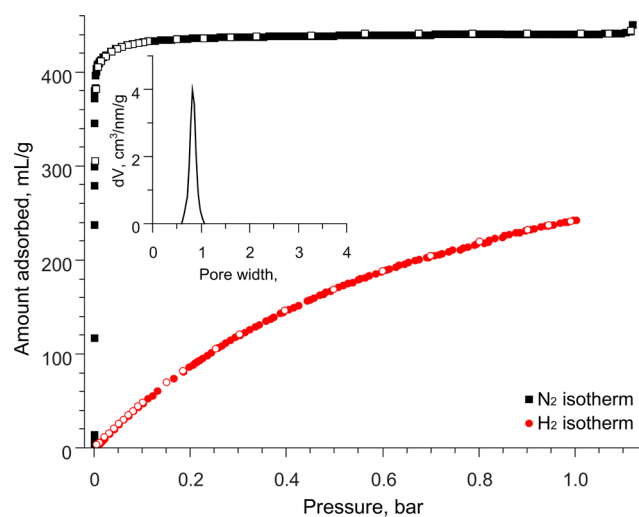


**Figure 4.**  $\text{N}_2$  (black squares) and  $\text{H}_2$  (red circles) isotherms for **1a** at 77 K: adsorption, full symbols; desorption, open symbols. Inset: pore size distribution curve.

PLATON SOLV routine.<sup>37</sup> This is entirely consistent with the complete activation of the material and the overall stability of the porous structure under these conditions. The pore-size distribution, calculated from the N<sub>2</sub> isotherm, gives a sharp peak near 8 Å, which corresponds to the van der Waals diameter of the cubic cages in **1a** (ca. 8–9 Å). The pore volume of **1a** and its specific surface area are very close to those reported earlier for the terephthalate analogue [Zn<sub>2</sub>(bdc)<sub>2</sub>dabco] (**4a**; 0.75 cm<sup>3</sup>·g<sup>-1</sup> and 1450 m<sup>2</sup>·g<sup>-1</sup>, respectively).<sup>38</sup> Consistent with these surface area data, the H<sub>2</sub> adsorption for **1a** (245 cm<sup>3</sup>·g<sup>-1</sup> and 2.23 wt % at 77 K and 1 bar) is slightly higher than that for **4a** (2.0 wt %) under similar conditions.

The reported CO<sub>2</sub> adsorption measurements for **4a**,<sup>39,40</sup> as well as our data (see the Supporting Information) indicate a moderate gas uptake of 9.0 wt % (46 cm<sup>3</sup>·g<sup>-1</sup>) at 298 K and 1 bar and of 23.9 wt % (122 cm<sup>3</sup>·g<sup>-1</sup>) at 273 K and 1 bar. In contrast, CO<sub>2</sub> adsorption in **1a**, which shows a porosity similar to that of **4a**, reveals a significant increase of ca. 50% in uptake under the same conditions. The maximum CO<sub>2</sub> adsorption in **1a** at 1 bar reaches 13.2 wt % (67.4 cm<sup>3</sup>·g<sup>-1</sup>) at 298 K and 30.0 wt % (153 cm<sup>3</sup>·g<sup>-1</sup>) at 273 K (Figure 5). At a pressure of 0.15 bar, which is relevant to the flue gas processing, the CO<sub>2</sub> uptakes of **1a** are 18.5 and 8.5 wt % at 273 and 298 K, respectively.

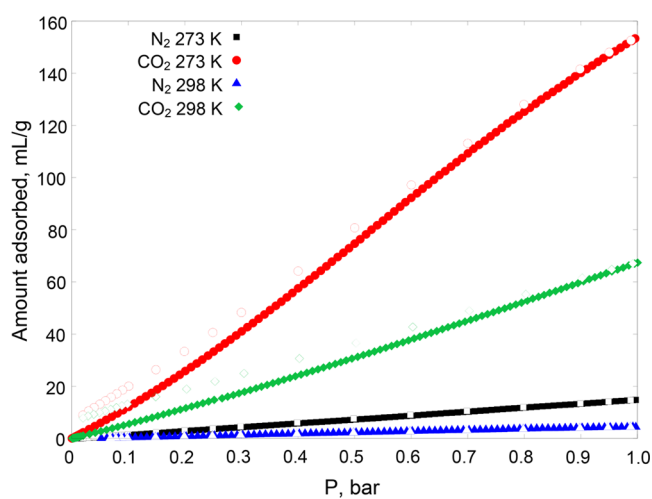


**Figure 5.** N<sub>2</sub> and CO<sub>2</sub> adsorption (full symbols) and desorption (open symbols) isotherms on **1a** at 273 and 298 K.

The isosteric heat of adsorption for CO<sub>2</sub> in **4a** at zero coverage, calculated from the isotherms at 273 and 298 K using the Clausius–Clapeyron equation, is 19.52 kJ·mol<sup>-1</sup>, consistent with the literature data.<sup>41</sup> The heat of adsorption of CO<sub>2</sub> for **1a** is noticeably higher at 23.65 kJ·mol<sup>-1</sup>, reflecting presumably stronger binding of CO<sub>2</sub> to the thiophene ring. The modest adsorption enthalpy of **1a** highlights the absence of strong binding centers in **1a**, with open metal sites and active amines reported to increase the heat of adsorption to 35–45 and 50–100 kJ·mol<sup>-1</sup>, respectively.<sup>5,6</sup> Despite the negative impact to the selectivity,<sup>42</sup> the low heat of adsorption in **1a** decreases the energy penalty for regeneration of the porous material in a temperature-swing process.

**Gas Adsorption Selectivity and Gas Separation Studies.** Together with CO<sub>2</sub> uptake, the CO<sub>2</sub>/N<sub>2</sub> adsorption selectivity is one of the most important parameters for the

practical application of porous materials in the purification of the industrial exhausts.<sup>43</sup> The adsorption data (see the Supporting Information) allowed us to calculate the CO<sub>2</sub>/N<sub>2</sub> selectivity factors for **1a** and **4a** at 298 K by three commonly used methodologies via (i) the ratio of the adsorbed gas volume, (ii) the ratio of the Henry's constants, and (iii) ideal adsorbed solution theory (IAST). The selectivity, calculated as the ratio of the adsorbed gas volumes by **1a** at 1 bar, is V(CO<sub>2</sub>)/V(N<sub>2</sub>) = 15.1 (Figure 5). By considering a typical flue gas composition of 0.15 bar of CO<sub>2</sub> and 0.75 bar of N<sub>2</sub>, the normalized<sup>37</sup> selectivity of adsorption at this composition can be calculated as S<sub>ads</sub> = 11.4. The corresponding numbers for **4a** are V(CO<sub>2</sub>)/V(N<sub>2</sub>) = 10.2 and S<sub>ads</sub> = 9.4. The Henry's constants (K<sub>H</sub>) were derived from the linear approximation of the low-pressure part of the isotherms, and on the basis of the obtained values of K<sub>H</sub> for **1a** and **4a** the selectivity factors at 298 K were calculated to be 12.5 and 8.9, respectively. The IAST<sup>44</sup> calculations for **1a** resulted in a selectivity factor of 11.2 for an equimolar CO<sub>2</sub>/N<sub>2</sub> mixture, while for **4a**, this factor is 9.2. Thus, a comparison of the above selectivity factors for **1a** and **4a** concludes that substitution of a phenyl group to thiophene upon going from **4a** to **1a** enhances the CO<sub>2</sub>/N<sub>2</sub> adsorption selectivity by 20–50%, depending on the methodology used. Finally, it is important to note that, even though the obtained selectivity factors for **1a** are lower than those for MOFs with strong CO<sub>2</sub> binding centers, a selectivity above 8 is high enough to be considered for practical applications.<sup>45</sup>

The potential of utilizing these MOFs for CO<sub>2</sub> separation has also been confirmed in breakthrough experiments in which an equimolar mixture of CO<sub>2</sub>/N<sub>2</sub> was flowed over a packed bed of **1a** at 298 K and 1.0 bar (Figure 6). To validate the role of the thiophene group in enhanced CO<sub>2</sub> binding, a corresponding

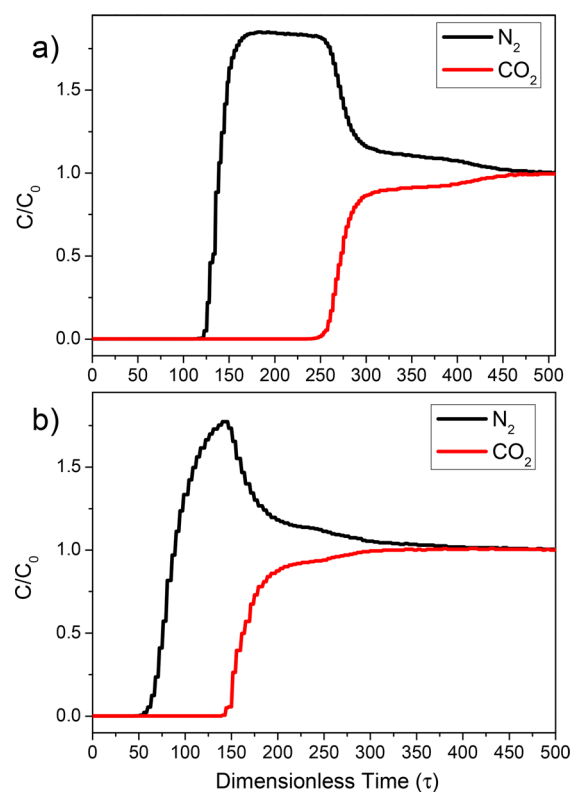


**Figure 6.** Dimensionless breakthrough curves for a N<sub>2</sub>/CO<sub>2</sub> mixture (1:1) for **1a** (a) and **4a** (b) at 25 °C and 1 bar.

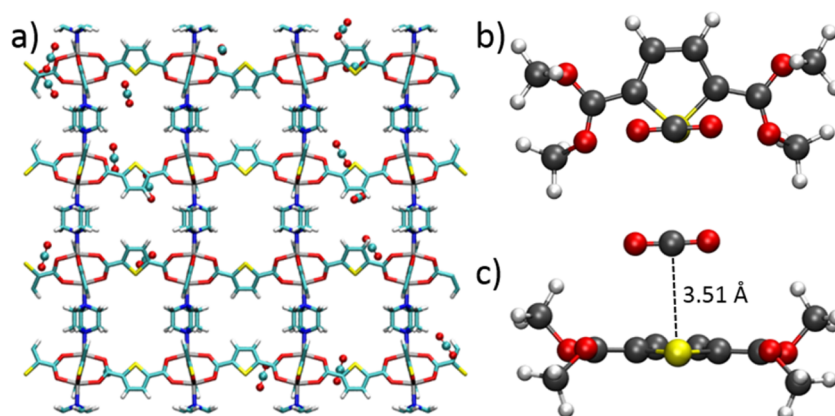


**Figure 7.** Snapshot from a GCMC simulation at low pressure in which the majority of CO<sub>2</sub> molecules were found to be located near to the thiophene ring (a). DFT-optimized lowest-energy binding sites for CO<sub>2</sub> viewed from above the tdc<sup>2-</sup> fragment (b and c).

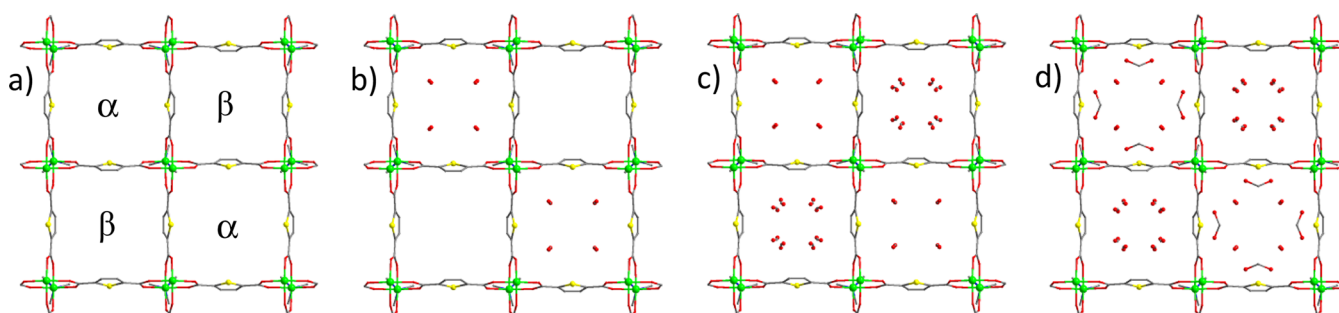


**Figure 8.** Single-crystal X-ray structures for **1a** as a function of the CO<sub>2</sub> loading (projection along the *c* direction): gas-free activated structure **1a** featuring sulfur-rich ( $\alpha$ ) and sulfur-poor ( $\beta$ ) channels, respectively (a); views of the binding sites for adsorbed CO<sub>2</sub> molecules at gradually increased population of CO<sub>2</sub> in the channels of **1a** (b–d).

breakthrough experiment has also been conducted on the phenyl-functionalized material **4a** under the same conditions. As predicted by the selectivity calculations, complete separation has been achieved in both cases, with N<sub>2</sub> being the first to elute through the bed while CO<sub>2</sub> was retained. Upon saturation, CO<sub>2</sub> breaks through from the bed and reaches saturation rapidly. As shown in Figure 6, dimensionless breakthrough plots offer a direct comparison between **1a** and **4a** on the performance of separation of the CO<sub>2</sub>/N<sub>2</sub> mixture. Significantly, **1a** shows a pronouncedly better separation than **4a** ( $\Delta\tau = 130$  and  $87$  for **1a** and **4a**, respectively). Additionally, the enhanced CO<sub>2</sub> storage capacity by thiophene functionalization in **1a** has been confirmed by delayed (by almost a factor of 2) breakthrough of CO<sub>2</sub> ( $\tau = 250$  and  $143$  for **1a** and **4a**, respectively). These results confirm the potential application of **1a** upon CO<sub>2</sub>/N<sub>2</sub> separation.

**Theoretical Studies.** Achieving such an outstanding affinity toward CO<sub>2</sub> in the absence of strong Lewis basic centers or coordinatively unsaturated metal sites prompted us to thoroughly investigate nature of the CO<sub>2</sub> binding in **1a**. The main difference between **1a** and **4a** is the chemical environment of the microporous surface as the channels in **1a** are decorated by sulfur atoms from the thiophene-2,5-dicarboxylate linkers. In the absence of any stronger intermolecular interactions (such as donor–acceptor bonds or hydrogen bonds), the CO<sub>2</sub> guest molecules have to interact with the porous host through somewhat weaker dipole–dipole interactions. The sulfur atom is more susceptible to polarization and to induced dipole interactions with the quadrupole of CO<sub>2</sub>. A comparison of [Zr<sub>6</sub>O<sub>4</sub>(OH)<sub>4</sub>(bpd<sub>6</sub>)<sub>6</sub>] with [Zr<sub>6</sub>O<sub>4</sub>(OH)<sub>4</sub>(bt<sub>6</sub>)<sub>6</sub>] (bpd<sup>2-</sup> =

biphenyl-4,4'-dicarboxylate; bt<sub>6</sub><sup>2-</sup> = bithiophenedicarboxylate) shows, depending on the temperature, a 32–78% increase of the gravimetric CO<sub>2</sub> uptake for the latter thiophene-containing structure.<sup>25</sup> It was suggested that differences in the electrostatic surface potentials for bpd<sup>2-</sup> and bt<sub>6</sub><sup>2-</sup> accounted for this difference, but no direct chemical explanation was given. In order to understand the role of the tdc<sup>2-</sup> ligand in CO<sub>2</sub> adsorption in **1a**, we undertook grand canonical Monte Carlo (GCMC) simulations (see the Supporting Information). These reveal unambiguously that CO<sub>2</sub> is preferentially adsorbed near the tdc<sup>2-</sup> linker at low loading (Figure 7a) and that thiophene plays a key role in the adsorption of CO<sub>2</sub> at low pressure. The CO<sub>2</sub>⋯tdc<sup>2-</sup> interaction was probed further by density functional theory (DFT) simulations, which confirmed that the C–S bond provides an excellent binding site for CO<sub>2</sub> (Figure 7b,c), with calculated binding energies ranging from  $-15.7$  to  $-18.3$  kJ·mol<sup>-1</sup>, ca. 3–10 kJ·mol<sup>-1</sup> stronger than those reported for CO<sub>2</sub> with benzene-based moieties.<sup>46–48</sup> The shortest S⋯C interatomic distance in the energy-optimized thiophene⋯CO<sub>2</sub> complex is 3.51 Å (Figure 7c), equal to the sum of the van der Waals radii of sulfur and carbon. The simulated heat of CO<sub>2</sub> adsorption in **1a** (24.2 kJ·mol<sup>-1</sup>) coincides with the experimental value (23.65 kJ·mol<sup>-1</sup>), giving consistency between the theory and experiment. The lower value of the heat of adsorption of CO<sub>2</sub> for **4a** (19.6 kJ·mol<sup>-1</sup>),<sup>39</sup> calculated by DFT, suggests and generalizes the idea that the inclusion of thiophene-based ligands in MOFs provides a route to materials with increased affinities for CO<sub>2</sub>.

**Determination of the Binding Sites for Adsorbed CO<sub>2</sub>.** We also sought to determine the preferred binding sites of

adsorbed CO<sub>2</sub> molecules in the extended pore structure of **1a** by in situ synchrotron single-crystal X-ray diffraction. A desolvated sample of **1a** shows complete retention of the framework structure and removal of the guest-free solvent molecules from the pore (Figure 8a). Two types of pores can be clearly observed and are denoted as  $\alpha$  and  $\beta$  with pore diameters of 7.1 and 7.8 Å (taking into consideration the van der Waals radii), respectively. The sulfur centers of all thiophene groups point into pore  $\alpha$ , whereas pore  $\beta$  is primarily functionalized with  $-\text{CH}$  moieties on the thiophene. The desolvated **1a** was then loaded with CO<sub>2</sub> at a pressure of 1.0 bar at 273 K and diffraction data collected at time  $t = 0.25$ , 1, and 2 h to capture the dynamic information on the site population. It is worth mentioning that the kinetics of gas uptake in single crystals can be different from that of the powder sample typically used in isotherm experiments. Analysis of the diffraction data indicates the absence of a notable structural phase change of **1a** upon CO<sub>2</sub> inclusion. Sequential Fourier difference map analysis of the diffraction data revealed the positions of the adsorbed CO<sub>2</sub> molecules in all three structures (Figure 8b–d).

At the first data set of CO<sub>2</sub>-loaded **1a**, only one binding site (CO<sub>2</sub><sup>I</sup>) was located within pore  $\alpha$  of **1a**·(CO<sub>2</sub>)<sub>0.40</sub>. CO<sub>2</sub><sup>I</sup> (occupancy = 0.20) is located near the {Zn<sub>2</sub>} paddlewheel stabilized by dipole interactions to the paddlewheel and hydrogen bonds to the  $-\text{CH}$  groups (Figure S6). Upon the second data collection, **1a**·(CO<sub>2</sub>)<sub>1.56</sub>, the occupancy of CO<sub>2</sub><sup>I</sup> increases to 0.43, accompanied by the appearance of a second binding site (CO<sub>2</sub><sup>II</sup>) with an occupancy of 0.352. CO<sub>2</sub><sup>II</sup> was located in pore  $\beta$  and is close to the thiophene group (Figure S7). Interestingly, the CO<sub>2</sub>–thiophene interatomic distance found in the X-ray diffraction data (3.49 Å) is highly consistent with that (3.51 Å) obtained in the DFT calculation. Upon additional equilibrium time ( $t = 2$  h) of **1a**·(CO<sub>2</sub>)<sub>1.63</sub>, the occupancies of CO<sub>2</sub><sup>I</sup> and CO<sub>2</sub><sup>II</sup> drop slightly to 0.38 and 0.29, respectively, indicating a redistribution of the adsorbed CO<sub>2</sub> molecules. The rest of the adsorbed CO<sub>2</sub> molecules fill into a third site (CO<sub>2</sub><sup>III</sup>) with an occupancy of 0.14 (Figure S8). CO<sub>2</sub><sup>III</sup> was found in pore  $\alpha$ , forming an intermolecular dipole interaction with CO<sub>2</sub><sup>I</sup> in a “T-shaped” manner. Additional diffraction data collection at  $t > 2$  h yielded the same crystal structures as that of **1a**·(CO<sub>2</sub>)<sub>1.63</sub>, indicating the presence of an adsorption equilibrium. Thus, two out of three CO<sub>2</sub> binding sites are found within the sulfur-rich pore  $\alpha$  of **1a**, confirming the critical role of this heteroatom functionalization in CO<sub>2</sub> adsorption. Indeed, the observation of a direct host–guest interaction between the thiophene and CO<sub>2</sub><sup>II</sup> represents the first experimental evidence of CO<sub>2</sub> binding to a sulfur-rich functional group in MOFs.

## CONCLUSIONS

Three isorecticular porous MOFs based on [Zn<sub>2</sub>(OOCR)<sub>4</sub>] paddlewheels, connected through thiophene-2,5-dicarboxylate moieties and nitrogen-donor linkers (L) [Zn<sub>2</sub>(tdc)<sub>2</sub>L], have been synthesized and characterized. Apart from some structural distortions, these frameworks are very similar to the prototypic zinc(II) terephthalate material [Zn<sub>2</sub>(bdc)<sub>2</sub>dabco] and have similar porosities in terms of the pore size, volume, and specific surface area. However, substitution of a phenyl group with thiophene substantially increases the adsorption of CO<sub>2</sub> as well as the CO<sub>2</sub>/N<sub>2</sub> separation selectivity, as is evidenced by thorough gas isotherm measurements and breakthrough experiments. The thiophene-lined **1a** possesses very good

CO<sub>2</sub> uptake under ambient conditions even though it features neither basic amine functions nor open metal sites, which is reflected by a low isosteric heat of adsorption. The in situ synchrotron X-ray diffraction data and quantum-chemical calculation confirm the role of the thiophene heterocycle and, particularly, sulfur atoms in binding CO<sub>2</sub> via induced dipole interactions. These results emphasize the feasibility of van der Waals interactions to effective CO<sub>2</sub> binding while maintaining low heat of adsorption within a hydrophobic porous material. More importantly, the incorporation of heterocycles into porous structures may represent a viable route to improving the adsorption properties of already-known materials.

## ASSOCIATED CONTENT

### Supporting Information

The Supporting Information is available free of charge on the ACS Publications website at DOI: 10.1021/acs.inorgchem.8b00138.

Details of the analytical methods, single-crystal X-ray diffraction experiments, gas adsorption measurements, GCMC and DFT calculations, and additional figures and plots (PDF)

### Accession Codes

CCDC 1503063–1503066 and 1568882–1568885 contain the supplementary crystallographic data for this paper. These data can be obtained free of charge via [www.ccdc.cam.ac.uk/data\\_request/cif](http://www.ccdc.cam.ac.uk/data_request/cif), or by emailing [data\\_request@ccdc.cam.ac.uk](mailto:data_request@ccdc.cam.ac.uk), or by contacting The Cambridge Crystallographic Data Centre, 12 Union Road, Cambridge CB2 1EZ, UK; fax: +44 1223 336033.

## AUTHOR INFORMATION

### Corresponding Authors

\*E-mail: [dan@niic.nsc.ru](mailto:dan@niic.nsc.ru).

\*E-mail: [M.Schroder@manchester.ac.uk](mailto:M.Schroder@manchester.ac.uk).

### ORCID

Laura J. M<sup>c</sup>Cormick: 0000-0002-6634-4717

Elena Besley: 0000-0002-9910-7603

Martin Schröder: 0000-0001-6992-0700

### Notes

The authors declare no competing financial interest.

## ACKNOWLEDGMENTS

We thank the EPSRC, ERC, and University of Manchester for funding. The NIIC team is grateful to the Russian Science Foundation (Grant 14-23-00013) and Federal Agency for Scientific Organizations for financial support. We thank the University of Nottingham for HPC facilities. M.S. acknowledges the Russian Ministry of Science and Education for the award of a Russian Megagrant (Grant 14.Z50.31.0006). We are especially grateful to the Advanced Light Source for access to Beamline 11.3.1. This research used resources of the Advanced Light Source, which is a DOE Office of Science User Facility under contract no. DE-AC02-05CH11231. The development of the gas cell used in this work was partially funded by the Center for Gas Separations Relevant to Clean Energy Technologies, an Energy Frontier Research Center funded by U.S. Department of Energy, Office of Science, Basic Energy Sciences, under Award DE-SC0001015.

## REFERENCES

- (1) Yuan, Z.; Eden, M. R.; Gani, R. Toward the development and deployment of large-scale carbon dioxide capture and conversion processes. *Ind. Eng. Chem. Res.* **2016**, *55*, 3383–3419.
- (2) Huck, J. M.; Lin, L.-C.; Berger, A. H.; Shahrak, M. N.; Martin, R. L.; Bhowan, A. S.; Haranczyk, M.; Reuter, K.; Smit, B. Evaluating different classes of porous materials for carbon capture. *Energy Environ. Sci.* **2014**, *7*, 4132–4146.
- (3) Zhang, Z.; Yao, Z.-Z.; Xiang, S.; Chen, B. Perspective of microporous metal–organic frameworks for CO<sub>2</sub> capture and separation. *Energy Environ. Sci.* **2014**, *7*, 2868–2899.
- (4) Lin, X.; Champness, N. R.; Schröder, M. Hydrogen, methane and carbon dioxide adsorption in metal-organic framework materials. *Top. Curr. Chem.* **2009**, *293*, 35–76.
- (5) Sumida, K.; Rogow, D. L.; Mason, J. A.; McDonald, T. M.; Bloch, E. D.; Herm, Z. R.; Bae, T.-H.; Long, J. R. Carbon dioxide capture in metal–organic frameworks. *Chem. Rev.* **2012**, *112*, 724–781.
- (6) Andriova, D.; Cogswell, C. F.; Lei, Y.; Choi, S. Effect of the structural constituents of metal organic frameworks on carbon dioxide capture. *Microporous Mesoporous Mater.* **2016**, *219*, 276–305.
- (7) Yu, J.; Xie, L.-H.; Li, J.-R.; Ma, Y.; Seminario, J. M.; Balbuena, P. B. CO<sub>2</sub> Capture and separations using MOFs: computational and experimental studies. *Chem. Rev.* **2017**, *117*, 9674–9754.
- (8) Li, J.-R.; Ma, Y.; McCarthy, M. C.; Sculley, J.; Yu, J.; Jeong, H.-K.; Balbuena, P. B.; Zhou, H.-C. Carbon dioxide capture–related gas adsorption and separation in metal–organic frameworks. *Coord. Chem. Rev.* **2011**, *255*, 1791–1823.
- (9) Liu, J.; Thallapally, P. K.; McGrail, B. P.; Brown, D. R.; Liu, J. Progress in adsorption-based CO<sub>2</sub> capture by metal–organic frameworks. *Chem. Soc. Rev.* **2012**, *41*, 2308–2322.
- (10) Belmabkhout, Y.; Guillerm, V.; Eddaoudi, M. Low concentration CO<sub>2</sub> capture using physical adsorbents: are metal-organic frameworks becoming the new benchmark materials? *Chem. Eng. J.* **2016**, *296*, 386–397.
- (11) McDonald, T. M.; Mason, J. A.; Kong, X.; Bloch, E. D.; Gygi, D.; Dani, A.; Crocellà, V.; Giordanino, F.; Odoh, S. O.; Drisdell, W. S.; Vlasisavljevič, B.; Dzubak, A. L.; Poloni, R.; Schnell, S. K.; Planas, N.; Lee, K.; Pascal, T.; Wan, L. F.; Prendergast, D.; Neaton, J. B.; Smit, B.; Kortricht, J. B.; Gagliardi, L.; Bordiga, S.; Reimer, J. A.; Long, J. R. Cooperative insertion of CO<sub>2</sub> in diamine-appended metal-organic frameworks. *Nature* **2015**, *519*, 303–308.
- (12) Martínez, F.; Sanz, R.; Orcajo, G.; Briones, D.; Yángüez, V. Amino-impregnated MOF materials for CO<sub>2</sub> capture at post-combustion conditions. *Chem. Eng. Sci.* **2016**, *142*, 55–61.
- (13) Li, L.-J.; Liao, P.-Q.; He, C.-T.; Wei, Y.-S.; Zhou, H.-L.; Lin, J.-M.; Li, X.-Y.; Zhang, J.-P. Grafting alkylamine in UiO-66 by charge-assisted coordination bonds for carbon dioxide capture from high humidity flue gas. *J. Mater. Chem. A* **2015**, *3*, 21849–21855.
- (14) Lee, W. R.; Jo, H.; Yang, L.-M.; Lee, H.; Ryu, D. W.; Lim, K. S.; Song, J. H.; Min, D. Y.; Han, S. S.; Seo, J. G.; Park, Y. K.; Moon, D.; Hong, C. S. Exceptional CO<sub>2</sub> working capacity in a heterodiamine-grafted metal–organic framework. *Chem. Sci.* **2015**, *6*, 3697–3705.
- (15) Lin, Y.; Kong, C.; Chen, L. Amine-functionalized metal–organic frameworks: structure, synthesis and applications. *RSC Adv.* **2016**, *6*, 32598–32614.
- (16) Luo, F.; Yan, C.; Dang, L.; Krishna, R.; Zhou, W.; Wu, H.; Dong, X.; Han, Y.; Hu, T.-L.; O’Keeffe, M.; Wang, L.; Luo, M.; Lin, R.-B.; Chen, B. UTSA-74: A MOF-74 isomer with two accessible binding sites per metal center for highly selective gas separation. *J. Am. Chem. Soc.* **2016**, *138*, 5678–5684.
- (17) Yan, Y.; Suyetin, M.; Bichoutskaia, E.; Blake, A. J.; Allan, D. R.; Barnett, S. A.; Schröder, M. Modulating the packing of [Cu<sub>24</sub>(isophthalate)<sub>24</sub>] cuboctahedra in a triazole-containing metal–organic polyhedral framework. *Chem. Sci.* **2013**, *4*, 1731–1736.
- (18) Yazaydin, A. Ö.; Snurr, R. Q.; Park, T.-H.; Koh, K.; Liu, J.; LeVan, M. D.; Benin, A. I.; Jakubczak, P.; Lanuza, M.; Galloway, D. B.; Low, J. J.; Willis, R. R. Screening of metal–organic frameworks for carbon dioxide capture from flue gas using a combined experimental and modeling approach. *J. Am. Chem. Soc.* **2009**, *131*, 18198–18199.
- (19) Alsmail, N. H.; Suyetin, M.; Yan, Y.; Cabot, R.; Krap, C. P.; Lü, J.; Easun, T. L.; Bichoutskaia, E.; Lewis, W.; Blake, A. J.; Schröder, M. Analysis of high and selective uptake of CO<sub>2</sub> in an oxamide-containing {Cu<sub>2</sub>(OOCR)<sub>4</sub>}<sub>n</sub>-based metal–organic framework. *Chem. - Eur. J.* **2014**, *20*, 7317–7324.
- (20) Zhou, D.-D.; He, C.-T.; Liao, P.-Q.; Xue, W.; Zhang, W.-X.; Zhou, H.-L.; Zhang, J.-P.; Chen, X.-M. A flexible porous Cu(II) bis-imidazolate framework with ultrahigh concentration of active sites for efficient and recyclable CO<sub>2</sub> capture. *Chem. Commun.* **2013**, *49*, 11728–11730.
- (21) Yuan, D.; Zhao, D.; Sun, D.; Zhou, H.-C. An isoreticular series of metal–organic frameworks with dendritic hexacarboxylate ligands and exceptionally high gas-uptake capacity. *Angew. Chem., Int. Ed.* **2010**, *49*, 5357–5361.
- (22) Yang, S.; Sun, J.; Ramirez-Cuesta, A. J.; Callear, S. K.; David, W. I. F.; Anderson, D. P.; Newby, R.; Blake, A. J.; Parker, J. E.; Tang, C. C.; Schröder, M. Selectivity and direct visualization of carbon dioxide and sulfur dioxide in a decorated porous host. *Nat. Chem.* **2012**, *4*, 887–894.
- (23) Plonka, A. M.; Banerjee, D.; Woerner, W. R.; Zhang, Z.; Nijem, N.; Chabal, Y. J.; Li, J.; Parise, J. B. Mechanism of Carbon Dioxide Adsorption in a Highly Selective Coordination Network Supported by Direct Structural Evidence. *Angew. Chem., Int. Ed.* **2013**, *52*, 1692–1695.
- (24) Ibarra, I. A.; Mace, A.; Yang, S.; Sun, J.; Lee, S.; Chang, J.-S.; Laaksonen, A.; Schröder, M.; Zou, X. Adsorption properties of MFM-400 and MFM-401 with CO<sub>2</sub> and hydrocarbons: selectivity derived from directed supramolecular interactions. *Inorg. Chem.* **2016**, *55*, 7219–7228.
- (25) Yoon, M.; Moon, D. New Zr (IV) based metal-organic framework comprising a sulfur-containing ligand: enhancement of CO<sub>2</sub> and H<sub>2</sub> storage capacity. *Microporous Mesoporous Mater.* **2015**, *215*, 116–122.
- (26) Nugent, P.; Belmabkhout, Y.; Burd, S. D.; Cairns, A. J.; Luebke, R.; Forrest, K.; Pham, T.; Ma, S.; Space, B.; Wojtas, L.; Eddaoudi, M.; Zaworotko, M. J. Porous materials with optimal adsorption thermodynamics and kinetics for CO<sub>2</sub> separation. *Nature* **2013**, *495*, 80–84.
- (27) Zhai, Q.-G.; Bu, X.; Mao, C.; Zhao, X.; Daemen, L.; Cheng, Y.; Ramirez-Cuesta, A. J.; Feng, P. An ultra-tunable platform for molecular engineering of high-performance crystalline porous materials. *Nat. Commun.* **2016**, *7*, 13645.
- (28) Gao, W.-Y.; Yan, W.; Cai, R.; Williams, K.; Salas, A.; Wojtas, L.; Shi, X.; Ma, S. A pillared metal–organic framework incorporated with 1,2,3-triazole moieties exhibiting remarkable enhancement of CO<sub>2</sub> uptake. *Chem. Commun.* **2012**, *48*, 8898–8900.
- (29) Gao, W.-Y.; Pham, T.; Forrest, K. A.; Space, B.; Wojtas, L.; Chen, Y.-S.; Ma, S. Local electric field favours more than exposed nitrogen atoms on CO<sub>2</sub> capture: a case study on the rht-type MOF platform. *Chem. Commun.* **2015**, *51*, 9636–9639.
- (30) Gao, Q.; Zhao, X.-L.; Chang, Z.; Xu, J.; Bu, X.-H. Structure stabilization of a metal-organic framework for gas sorption investigation. *Dalton Trans.* **2016**, *45*, 6830–6833.
- (31) Ren, G.-J.; Liu, Y.-Q.; Hu, T.-L.; Bu, X.-H. Two robust metal-organic frameworks with uncoordinated N atoms for CO<sub>2</sub> adsorption. *CrystEngComm* **2015**, *17*, 8198–8201.
- (32) Zhang, D.-S.; Chang, Z.; Li, Y.-F.; Jiang, Z.-Y.; Xuan, Z.-H.; Zhang, Y.-H.; Li, J.-R.; Chen, Q.; Hu, T.-L.; Bu, X.-H. Fluorous metal-organic frameworks with enhanced stability and high H<sub>2</sub>/CO<sub>2</sub> storage capacities. *Sci. Rep.* **2013**, *3*, 3312.
- (33) M, P.; Asha, K. S.; Sinha, M.; Poduval, A.; Mandal, S. The structural diversity, band gap energy and photoluminescence properties of thiophenedicarboxylate based coordination polymers. *CrystEngComm* **2016**, *18*, 536–543.
- (34) Dybtsev, D. N.; Sokolov, I. E.; Peresypkina, E. V.; Fedin, V. P. Design of scaffold-like metal-organic coordination polymers based on dinuclear zinc(II) carboxylate complexes. *Russ. Chem. Bull.* **2007**, *56*, 225–230.

(35) Dybtsev, D. N.; Chun, H.; Kim, K. Rigid and Flexible: A highly porous metal–organic framework with unusual guest-dependent dynamic behavior. *Angew. Chem., Int. Ed.* **2004**, *43*, 5033–5036.

(36) Kim, Y.; Haldar, R.; Kim, H.; Koo, J.; Kim, K. The guest-dependent thermal response of the flexible MOF  $Zn_2(\text{BDC})_2(\text{DABCO})$ . *Dalton Trans.* **2016**, *45*, 4187–4192.

(37) Spek, A. L. Structure validation in chemical crystallography. *Acta Crystallogr., Sect. D: Biol. Crystallogr.* **2009**, *65*, 148–155.

(38) Chun, H.; Dybtsev, D. N.; Kim, H.; Kim, K. Synthesis, X-ray crystal structures, and gas sorption properties of pillared square grid nets based on paddle-wheel motifs: implications for hydrogen storage in porous materials. *Chem. - Eur. J.* **2005**, *11*, 3521–3529.

(39) Chen, Z.; Xiang, S.; Zhao, D.; Chen, B. Reversible two-dimensional–three dimensional framework transformation within a prototype metal–organic framework. *Cryst. Growth Des.* **2009**, *9*, 5293–5296.

(40) Chen, Z.; Xiang, S.; Arman, H. D.; Li, P.; Zhao, D.; Chen, B. Significantly enhanced  $\text{CO}_2/\text{CH}_4$  separation selectivity within a 3D prototype metal–organic framework functionalized with OH groups on pore surfaces at room temperature. *Eur. J. Inorg. Chem.* **2011**, *2011*, 2227–2231.

(41) Burtch, N. C.; Jasuja, H.; Dubbeldam, D.; Walton, K. S. Molecular-level insight into unusual low pressure  $\text{CO}_2$  affinity in pillared metal–organic frameworks. *J. Am. Chem. Soc.* **2013**, *135*, 7172–7180.

(42) Mason, J. A.; Sumida, K.; Herm, Z. R.; Krishna, R.; Long, J. R. Evaluating metal–organic frameworks for post-combustion carbon dioxide capture via temperature swing adsorption. *Energy Environ. Sci.* **2011**, *4*, 3030.

(43) Krishna, R. Methodologies for evaluation of metal–organic frameworks in separation applications. *RSC Adv.* **2015**, *5*, 52269–52295.

(44) Myers, A. L.; Prausnitz, J. M. Thermodynamics of mixed-gas adsorption. *AIChE J.* **1965**, *11*, 121–127.

(45) Duan, J.; Higuchi, M.; Krishna, R.; Kiyonaga, T.; Tsutsumi, Y.; Sato, Y.; Kubota, Y.; Takatae, M.; Kitagawa, S. High  $\text{CO}_2/\text{N}_2/\text{O}_2/\text{CO}$  separation in a chemically robust porous coordination polymer with low binding energy. *Chem. Sci.* **2014**, *5*, 660–666.

(46) Torrisi, A.; Bell, R. G.; Mellot-Draznieks, C. Predicting the impact of functionalized ligands on  $\text{CO}_2$  adsorption in MOFs: A combined DFT and Grand Canonical Monte Carlo study. *Microporous Mesoporous Mater.* **2013**, *168*, 225–238.

(47) Torrisi, A.; Mellot-Draznieks, C.; Bell, R. G. Impact of ligands on  $\text{CO}_2$  adsorption in metal-organic frameworks: First principles study of the interaction of  $\text{CO}_2$  with functionalized benzenes. II. Effect of polar and acidic substituents. *J. Chem. Phys.* **2010**, *132*, 044705.

(48) Besnard, M.; Cabaco, M. I.; Talaga, D.; Danten, Y. Vibrational energy transfer and anisotropy decay in liquid water: Is the Förster model valid? *J. Chem. Phys.* **2008**, *129*, 224511.